

Technical University of Denmark



Low temperature vibrational spectra, lattice dynamics, and phase transitions in some potassium hexahalometallates: $K_2[XY_6]$ with $X=Sn$ or Te and $Y=Cl$ or Br

Chodos, Steven L.; Berg, Rolf W.

Published in:
Journal of Chemical Physics

Link to article, DOI:
[10.1063/1.437378](https://doi.org/10.1063/1.437378)

Publication date:
1979

Document Version
Publisher's PDF, also known as Version of record

[Link back to DTU Orbit](#)

Citation (APA):
Chodos, S. L., & Berg, R. W. (1979). Low temperature vibrational spectra, lattice dynamics, and phase transitions in some potassium hexahalometallates: $K_2[XY_6]$ with $X=Sn$ or Te and $Y=Cl$ or Br . *Journal of Chemical Physics*, 70(11), 4864-4871. DOI: 10.1063/1.437378

DTU Library
Technical Information Center of Denmark

General rights

Copyright and moral rights for the publications made accessible in the public portal are retained by the authors and/or other copyright owners and it is a condition of accessing publications that users recognise and abide by the legal requirements associated with these rights.

- Users may download and print one copy of any publication from the public portal for the purpose of private study or research.
- You may not further distribute the material or use it for any profit-making activity or commercial gain
- You may freely distribute the URL identifying the publication in the public portal

If you believe that this document breaches copyright please contact us providing details, and we will remove access to the work immediately and investigate your claim.

Low temperature vibrational spectra, lattice dynamics, and phase transitions in some potassium hexahalometallates: $K_2[XY_6]$ with $X = \text{Sn}$ or Te and $Y = \text{Cl}$ or Br

Steven L. Chodos

Hughes Aircraft Company, Culver City, California 90230

Rolf W. Berg

Chemistry Department A, The Technical University of Denmark, DK-2800 Lyngby, Denmark

(Received 19 December 1978)

This paper deals with the observation and identification of phonon frequencies resulting from the low temperature phase transitions in K_2XY_6 crystals. By means of a simple lattice dynamical model, the vibrational Raman and IR data available in the literature and obtained here have been analyzed. The model used is an extension of one previously used to explain the vibronic spectra of several related compounds.

INTRODUCTION

Many crystals of the composition $K_2[XY_6]$, with $X = \text{metal (IV)}$ and $Y = \text{halogen}$, tend to adopt the cubic antiferroite ($K_2[\text{PtCl}_6]$ -type) structure with space group $Fm\bar{3}m$ (O_h^5) at higher temperatures. During cooling, these crystals sometimes transform, via second order phase transitions, to lower symmetry pseudocubic structures. Well-investigated examples are the $K_2[\text{ReCl}_6]$ and $K_2[\text{SnCl}_6]$ crystals, which have four transitions, the first of which is considered^{1,2} to originate from a condensation of a soft $[XY_6]$ rotary mode at the zone center Γ , transforming the crystal symmetry to $I4/m$ (C_{4h}^5) at 110.9 K for Re and to $P4/mnc$ (D_{4h}^5) at 261 K for Sn.

The crystals $K_2[\text{SnCl}_6]$ and $K_2[\text{SnBr}_6]$ are known to be rigorously cubic $Fm\bar{3}m$ (O_h^5) at higher temperatures. At the temperatures T_{c1} , these crystals transform to tetragonal phases, which are stable in a relatively narrow temperature range (see Table I). After passing below the second transformation temperature T_{c2} , these crystals turn into a third phase, which is known to be monoclinic for $K_2[\text{SnCl}_6]$.²

The $K_2[\text{TeCl}_6]$ crystal is monoclinic, though very nearly cubic, at room temperature. There is DTA indi-

cations of phase transitions at 332 and 339 K,⁸ but it has not yet been proved that the high temperature phase is cubic O_h^5 , as can be expected.

The situation in the $K_2[\text{TeBr}_6]$ crystal is almost the same: It is monoclinic¹⁵ at room temperature and also has transitions at higher temperatures (434 and 405 K),⁸ as well as a transition at 243 K, indicated by nuclear quadrupole experiments.¹⁴

It has been suggested¹ that the tetragonal and monoclinic structures are obtained as the result of small rotations of the $[XY_6]$ octahedra around one or another set of axes. To illustrate this, consider the very well-examined^{2,15} distortions present in the monoclinic phase III of $K_2[\text{SnCl}_6]$ or $K_2[\text{TeBr}_6]$. Basically, it is the cubic antiferroite lattice, but the following perturbations occur¹⁵:

(i) a rotation of neighboring regular octahedra about the c axis by $\sim 8^\circ$ for $[\text{SnCl}_6]$ and $\sim 12^\circ$ for $[\text{TeBr}_6]$, in alternating directions ("antiferro" rotations),

(ii) a "ferro" rotation of all octahedra about the monoclinic b axis (cubic $[110]$) by $\sim 8^\circ$ and 9° in the same direction, followed by

(iii) displacements of K^+ ions and small adjustments

TABLE I. Phase transitions of $K_2[XY_6]$ crystals. The known space groups and conversion temperatures (K) are indicated.

	Phase I (high temp.)	T_{c1}	Phase II	T_{c2}	Phase III
$K_2[\text{SnCl}_6]$ (Refs. 2-8)	$Fm\bar{3}m$ (O_h^5)	261	$P4/mnc$ (D_{4h}^6)	254	$P2_1/n$ (C_{2h}^5)
$K_2[\text{SnBr}_6]$ (Refs. 5-11)	$Fm\bar{3}m$ (O_h^5)	400	Tetragonal	375 ^b	lower than tetragonal; (Ref. 6) D_4^2 (Refs. 9 and 10)
$K_2[\text{TeCl}_6]^a$ [Refs. 8 and 12-14]	$Fm\bar{3}m$?	339	?	332	$C2/m$ (C_{2h}^3)
$K_2[\text{TeBr}_6]$ (Refs. 8, 14 and 15)	$Fm\bar{3}m$?	434	?	405	$P2_1/n$ (C_{2h}^5)

^aA transition to a fourth phase stable below ~ 165 K has been suggested.¹³

^bSwanson¹¹ has 368 ± 5 K.

of cell parameters.

The $K_2[TeCl_6]$ crystal structure at room temperature¹² is simpler than that of $K_2[TeBr_6]$, as the former lacks the distortion type (i). However, based on the low temperature infrared and Raman Spectra, it has been suggested¹³ that $K_2[TeCl_6]$ has a phase transition near $\sim 165 \pm 30$ K that results in some kind of unit cell multiplication.

On the other hand, the lower temperature phases of $K_2[ReCl_6]$ and $K_2[SnCl_6]$ are quite simple in that the type (i) antiferro rotations occur, but here without simultaneous type (ii) ferro rotations.

In 1970, O'Leary and Wheeler¹ established their lattice dynamical model for $K_2[ReCl_6]$, a model which quite successfully accounts for the observed low-temperature Raman and infrared spectral bands as well as analyzes the possible character of the phase transitions.

With their success in mind, it is tempting to try to construct and fit a similar model based on lattice dynamics for the $K_2[SnY_6]$ and $K_2[TeY_6]$ crystals, and this is done in the present paper. However, the situation here is slightly more difficult due to the initial monoclinic distortion in some of the crystals at room temperature, a feature which allows additional spectroscopic transitions to be observed. While this would normally be an advantage, the reduced symmetry also leads to splitting of degenerate "cubic" states. A simple lattice model based on octahedral symmetry alone will not be able to fit the additional bands resulting from the removal of the degeneracy. However, if the splitting is small, it may still be possible to use such a model to gain at least a qualitative understanding of the observed spectra.

EXPERIMENTAL

Experimental methods

Some missing experimental data concerning low temperature far IR and Raman spectra are provided in this section.

The compounds were prepared by standard methods: Freshly distilled pure $TeCl_4$ and pure KCl were melted in equivalent amounts in silica ampoules, limiting the reaction with atmospheric moisture using dry-box techniques; $SnCl_4$, $SnBr_4$, or TeO_2 were dissolved in the corresponding concentrated acid and mixed with KCl or KBr aqueous solutions. The purities of the compounds were tested by volumetric analysis of halogen:

	calc	found
K_2SnCl_6	51.932%	$51.2\% \pm 0.3\%$
K_2SnBr_6	70.889%	$70.9\% \pm 0.3\%$
K_2TeCl_6	50.826%	$51.2\% \pm 0.3\%$
K_2TeBr_6	69.967%	$68.8\% \pm 0.3\%$

The methods used in obtaining the spectra have been described in detail.¹³ The interferometric far IR technique was improved in two ways: (i) The heat conductivity of pressed discs of polyethylene was helped by covering the surface with paraffin oil and pressing onto

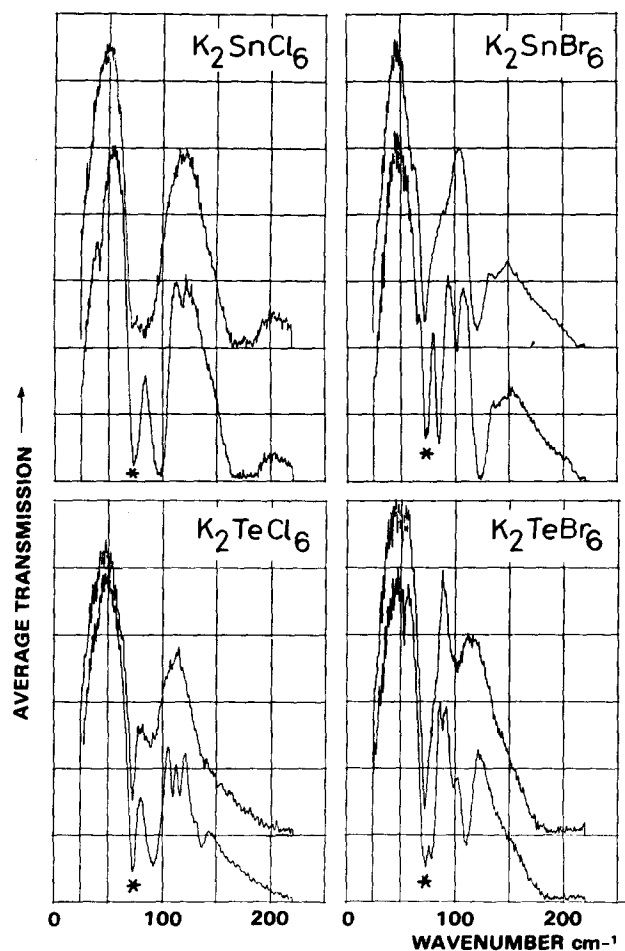


FIG. 1. Far infrared transmission spectra of $K_2[XY_6]$ obtained at room temperature (upper spectra) and at ~ 100 K. Resolution: 0.7 cm^{-1} . Finely dispersed powder in pressed polyethylene discs. The band at 72 cm^{-1} (marked with asterisk) is due to polyethylene.

a transparent silicon plate (from TOPSIL, Inc., Frederikssund, Denmark) in good contact along the whole periphery with the variably cold junction of the cryostat. The temperature was determined by an iron-constantan thermocouple. (ii) The double sided interferograms were corrected for drift and apodized using a squared sinus function prior to Cooley-Tukey fast Fourier transformation, done in a large computer with plotting facilities. Two or more spectra were finally averaged.

The true temperatures in the Raman experiments were estimated by recording the ν_5 mode on both the Stokes and anti-Stokes side and calculating the temperature from the ratio of integrated intensity, assuming Boltzmann's distribution. The temperatures determined in this way were reproducible within ± 10 K and were in general a few degrees higher than the copper block of the cryostat.

Experimental results

The results of the experimental work are shown in Figs. 1 and 2 and in Table II. Some seven phonon frequencies can be considered as well established, and various hypothetical assignments for some of the rest

TABLE II. Experimental Raman and IR absorption data (cm^{-1}) for $\text{K}_2[\text{XY}_6]$ at 300 K or as indicated, in (approximately) cubic space group $O_h^5 \equiv Fm\bar{3}m$.

	K_2SnCl_6	K_2SnBr_6	K_2TeCl_6	K_2TeBr_6	Possible identifications based on this work					
Lattice constant (\AA)	9.98	~ 10.54	~ 10.14	10.69						
X-Y bond length (\AA)	2.407	~ 2.63	~ 2.54	2.71						
Raman	Well-established origin			469, 465 ^c						
	$A_{1g}(\Gamma_1^+, \nu_1)$	324, 323.7 ^a	190, 190	297, 294 ^c	176, 177 ^c	$A_{1g}(\Gamma_1^+, \nu_1)$				
	$E_g(\Gamma_3^+, \nu_2)$	244, 245.8 ^a	144, 144	251, 251 ^c	154, 157 ^c	$E_g(\Gamma_3^+, \nu_2)$				
	$T_{2g}(\Gamma_5^+, \nu_3)$		177 ^a	116 ^e	149 ^c	99, 111 ^c	$(X_3^+, \nu_5 \text{ LO})$			
		172, 172 ^a	109, ^d	110 ^e	142 { 144 ^c	92, 103 ^c	$T_{2g}(\Gamma_5^+, \nu_3)$			
			164 ^a			137 ^c	X_5^+			
			104.4 ^a		109, 110 ^c		$T_{1g}+X_4^+$?			
			96.6 ^a	88 ^e	101 ^c		$T_{1g}+X_5^+$?			
	$T_{2g}(\Gamma_5^+, \nu_L)$				84 ^c		$T_{1g}+T_{1g}$?			
		$\sim 72,$	81.0 ^a	82, ^d	80 ^e	70 { 76 ^c	$T_{2g}(\Gamma_5^+, \nu_L)$			
			84.5 ^a		75 ^e	72 ^c	74, 74 ^c	X_5^+		
		54 ^b {	69.8 ^a	64, ^f	57 ^e	68 ^c		$T_{1g}(X_4^-)$		
			60.0 ^a	41, ^d	47 ^e	59, 60 ^c	48 ^c	$T_{1g}(X_5^-)$		
			46.3 ^a			48, 47 ^c		T_{1g}		
			37.8 ^a	23, ^d	33 ^e	36, 38 ^c	34 ^c			
Infrared			285, 288 ^c	312, 312 ^c						
	$T_{1u}(\Gamma_4^-, \nu_3)$	~ 324 (TO: 314)	$\sim 225,$	$\sim 225^c$	$\sim 255,$	~ 255	$\sim 195,$	$\sim 195^c$	$T_{1u}(\Gamma_4^-, \nu_3)$	
	$T_{1u}(\Gamma_4^-, \nu_4)$	~ 175	$\sim 121,$	124 ^c	140, 136 ^c	100, 110 ^c			$T_{1u}(\Gamma_4^-, \nu_4)$	
			118 ^c		128 ^c				X_5^-	
				101 ^c	115 ^c				$T_{2u}(X_5^-)$	
		97 ^c			109 ^c				$T_{2u}(\Gamma_5^-)$	
						100 ^c			$X_4^+ + X_4^-$?	
	$T_{1u}(\Gamma_4^-, \nu_L)$						89 ^c			X_5^-
		84	74.8 ^c	78, 84 ^c	87, 97 ^c	92 ^c	76, 79 ^c			X_3^-
						87 ^c				$T_{1u}(\Gamma_4^-, \nu_L)$
					57 ^c				X_5^-	
	42.5 ^c		65 ^c						X_2^-	
						53 ^c			X_4^-	
							53 ^c		$T_{1g}+X_5^-$	
									X_5^-	
References	4	11, 19	13	19, 20						

^aAt ~ 50 K.^bExtrapolated to ~ 300 K.^cAt ~ 100 K.^dAt ~ 300 K.¹¹^eAt ~ 95 K.¹¹^fAt 300 K.⁹

can be guessed and tested by the subsequent calculations. All four systems have been studied before, but not all at lower temperatures.^{3,4,11,13,20} The (reversible) evolution in the far IR spectra as the temperature is lowered

towards ~ 100 K shows the following:

(i) $\text{K}_2[\text{SnCl}_6]$: weak, narrow bands appear near 42.5 and 118 cm^{-1} at temperatures around ~ 200 K. These

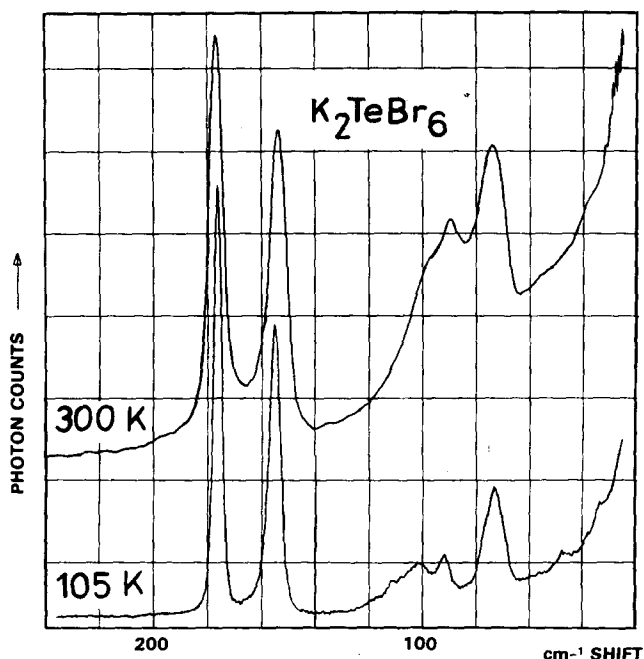


FIG. 2. Raman scattering spectra of $K_2[TeBr_6]$ power obtained at the indicated temperatures. Resolution: 2 cm^{-1} . Excited with $\sim 20\text{ mW}$ of filtered 16355 cm^{-1} dye laser radiation.

bands were stationary within experimental accuracy and disappeared reversibly by heating.

(ii) $K_2[SnBr_6]$: at $\sim 240\text{ K}$, a distinct shoulder emerges at $\sim 92\text{ cm}^{-1}$, moving to $\sim 101\text{ cm}^{-1}$, and gaining in intensity by cooling to $\sim 100\text{ K}$. At this temperature, weak bands at 199 and 65 cm^{-1} are seen, and all features show reversibility.

(iii) $K_2[TeCl_6]$: two pronounced bands at 115 and 109 cm^{-1} appear and disappear reversibly around 165 K . In some spectra (but not in all), we observed weak bands at 57 and 42 cm^{-1} at low temperatures.

(iv) $K_2[TeBr_6]$: there is a gradual evolution in the sharpness of bands by cooling. The 53 cm^{-1} band is faintly observable at room temperature. The 89 and

100 cm^{-1} bands can be weakly discerned around 200 K and are distinct only below $\sim 120\text{ K}$. ν_4 shifts $+10\text{ cm}^{-1}$. The changes are reversible. Adams *et al.*²⁰ observed ν_4 at 113 cm^{-1} and the band at 55 cm^{-1} at 120 K but did not resolve the bands at 100 and 89 cm^{-1} .

The Raman spectra of three of the salts as a function of temperature are given in Refs. 3, 4, 11, 13. Characteristically, at low temperatures, all four salts show faint bands in the range below 110 cm^{-1} and broad $T_{2g}(\Gamma_5^+, \nu_5)$ bands (Table II and Fig. 2).

These spectral features at low temperatures must be associated with the phase transitions (Table I). It seems to be a general rule that the new spectral features do not necessarily appear immediately below the transformation point but must await a considerable distortion of the structure. As an example, in $K_2[SnBr_6]$ with $T_{c2} = 375\text{ K}$, a lot of change is observed in the IR spectra between room temperature (300 K) and 100 K (Fig. 1). However, it is difficult to exclude a further transition to a phase IV ($K_2[ReCl_6]$ has a $T_{c3} = 76\text{ K}$), but at least in the Sn salts no indications of a T_{c3} has been seen using several different techniques.²⁻¹¹

Lattice dynamical calculation

The lattice dynamical model used to generate the phonon dispersion curves for the compounds considered here is similar to the model used for Cs_2UBr_6 ¹⁶ and Cs_2MnF_6 .^{17,18} Like O'Leary and Wheeler's model,¹ it is based on a parameterized force field acting between rigid ions. The model used here is characterized by a modified Urey-Bradley force field to describe the short range interactions within the XY_6 complex plus additional short range terms to characterize the interactions with the potassium lattice and adjacent XY_6 complexes. Added to this are the standard long range Coulomb terms.

A major problem with models of this type is to keep the number of adjustable parameters at a reasonably low level. Equation (1) gives the short range potential ϕ^{SR} in terms of internal bond coordinates out to second nearest neighbor intercell Y-Y interactions:

$$\begin{aligned} 2\phi^{SR} = & K \sum_I (\Delta r_i)^2 + F \sum_{II} (\Delta r_{ij})^2 + Hr_0^2 \sum_{III} (\Delta \theta_{ijk})^2 \\ & + K_2 \sum_{IV} (\Delta r_{ik})^2 + K_3 \sum_V (\Delta r_{ii})^2 + K_4 \sum_{VI} (\Delta r_{im})^2 + K_{rr} \sum_{VII} (\Delta r_i)(\Delta r_j) + K_5 \sum_{VIII} (\Delta r_{kk'})^2 + K_{\theta\theta} \sum_{IX} (\Delta \theta_{ijk})(\Delta \theta_{ijm}) \\ & + 2r_0 f' \sum_I (\Delta r_i) + 2R_1 F' \sum_{II} (\Delta r_{ij}) + 2R_2 k_2 \sum_{IV} (\Delta r_{ik}) + 2R_3 k_3 \sum_V (\Delta r_{ii}) + 2R_4 k_4 \sum_{VI} (\Delta r_{im}) + 2R_5 k_5 \sum_{VIII} (\Delta r_{kk'}), \end{aligned} \quad (1)$$

where the sums run over I = X-Y pairs, separated by r_i ; II = Y-Y nearest neighbor pairs in same complex, separated by r_{ij} ; III = Y-X-Y angles θ_{ijk} ; IV = K-Y nearest neighbor pairs, at r_{ik} ; V = Y-Y intercell nearest neighbor pairs, at r_{ii} ; VI = Y-Y intercell next nearest neighbor pairs, at r_{im} ; VII = *trans*-X-Y bonds; VIII = K-K nearest neighbor pairs, at $r_{kk'}$; IX = Y-X-Y angles with a common side; and where Δ denote change from equilibrium values, which are r_0 for the X-Y bond, R_1

for the Y-Y nearest neighbor distance $=\sqrt{2}r_0$, R_2 for the K-Y distance $\geq \sqrt{2}r_0$, R_3 for the Y-Y intercell nearest distance $\geq \sqrt{2}r_0$, R_4 for the second neighbor intercell Y separation $2r_0$, and R_5 for the K-K distance $\geq 2r_0$. The cell referred to here is the cube defined by the K ions, surrounding $[XY_6]^{2-}$.

The linear terms in Eq. (1) appear since the internal coordinates chosen are not independent. These terms

are related to the "perpendicular" force constants of O'Leary and Wheeler.¹ In equilibrium, forces on any atom must vanish. This is true by symmetry for all but the Y atoms. If we differentiate the total potential $\phi^{\text{SR}} + V^{\text{Coul}}$ with respect to the Y position coordinates, the result must equal zero. This gives the following relation between the linear short range terms (assuming that the Y's are at the center of the face formed by the K atoms):

$$f' + 4(F' - k_3) = -\frac{\delta V^{\text{Coul}}}{\delta Y_Y} \quad (2)$$

where $\delta V^{\text{Coul}}/\delta X_Y$ is the space derivative of the Coulomb part of the potential with respect to the Y atom. This last term was evaluated using Ewalds theta function transformation with the atomic charges as parameters, these being related by

$$2q_K + q_X - 6q_Y = 0.$$

Previously, in an effort to reduce the number of parameters, the short range interaction between halogen atoms Y in adjacent complexes was neglected. Except for the Coulomb terms, all of the intercell interactions in these models was conveyed by the quadratic K-Y interaction parameter K_2 .

The effect of this procedure has been to limit the dispersion and to affect the position of the T_{1g} mode.

The effect on dispersion of neglecting some of the intercell constants is illustrated by the second nearest neighbor linear Y-Y intercell parameter (k_4). An interesting effect of this force constant is that it allows a splitting of T_{1g} and X_4^+ . It is the only constant that does this. Because of its neglect, the T_{1g} and X_4^+ modes will always be nearly degenerate in our model. This is in contrast to the findings of O'Leary and Wheeler, and emphasizes the effect of the second nearest neighbor Y-Y intercell coupling. The X_4^+ mode is of particular interest since it has been identified as one of the soft modes in the $K_2[\text{ReCl}_6]$ system.¹

The T_{1g} mode is rather sensitive to the parameters of the model, and difficulties with it have been noted before. Additional freedom in fitting this mode is gained by adding either the linear K-Y interaction parameter k_2 or adding the quadratic Y-Y second nearest neighbor intercell parameter K_4 . These two parameters allow the T_{1g} mode to be moved relative to the other Γ point modes. We have chosen to only use K_4 as it has the least effect on the other $k=0$ modes. It should be noted that the nearest neighbor intercell Y-Y parameters (K_3, k_3) do not help in fitting any $k=0$ mode as they enter all modes in a linear combination with the Y-Y nearest neighbor intracell parameters (F, F') as $F + K_3$ and $F' + k_3$. This is to be expected since, for the halogen positions assumed, we are just adding the two "springs" in series for the $k=0$ modes. More importantly, the nearest neighbor intercell Y-Y distance does not change during a T_{1g} displacement. Because of this, these parameters were not used.

The parameter K_{rr} was retained because it aids in fitting the internal bond stretching modes of the $[\text{XY}_6]$ complex (A_{1g}, E_g , and the highest T_{1u}). The parameter $k_{\theta\theta}$ is sometimes added to the Urey-Bradley force field

to help in fitting the internal bending modes in the $[\text{XY}_6]$ complex (T_{2g}, T_{2u} , and second T_{1u}). However, it was not needed for the compounds considered here. The parameters F', k_2 , and $k_{\theta\theta}$ tend to cause deviation from the well-known $\nu_8 = \nu_5/\sqrt{2}$ result of the simple valence force field.

In this work, we have eliminated the following parameters: the nearest neighbor intercell Y-Y interaction (K_3, k_3); the linear Y-Y second nearest neighbor intercell interaction (k_4); the linear K-K interaction (k_5); and $K_{\theta\theta}$ and k_2 . f' was calculated by Eq. (2). This leaves 10 parameters. While all 10 parameters were used in fitting $K_2\text{TeCl}_6$, only eight were used for the other compounds. This was accomplished by fixing $F' = -0.1F$ and $q_K = 1.0$.

DISCUSSION OF LATTICE DYNAMICAL MODEL CALCULATIONS

General

The procedure used in fitting the parameters of the model was to start with selected "well established" modes. These were generally the $k=0$, room temperature modes which could usually be established by the systematics of these compounds. These are given in the left hand column of Table II. Based on these initial fittings, zone boundary phonons were identified that corresponded to the additional bands of the low temperature structure. As a check on the method, only $k=0$ modes and odd phonons at the point X (i.e., the additional IR data) were used in fitting the parameters of the model. The even phonons at X could then be calculated and compared to the additional low temperature Raman data.

Tables III and IV give the results of several attempts at fitting the four compounds considered here. Figure 3(a)-3(d) show the calculated dispersion curves. For clarity, only the phonons below 200 cm^{-1} are displayed. The dynamical matrix was diagonalized only at the points Γ, X , and L in the Brillouin zone. The dispersion curves along Δ and Λ are only approximate, being estimated from compatibility conditions and from the noncrossing of phonon branches of the same symmetry.

$K_2[\text{SnCl}_6]$

The Raman spectra of this compound have been investigated by Pelzl *et al.*⁴ in the neighborhood of the structural phase transitions. Their temperature dependent data show two soft modes that were identified as the Γ and X point rotational mode (T_{1g} and X_4^+). Additional low frequency bands ($105\text{--}38 \text{ cm}^{-1}$) appearing below the transition temperature were observed and associated with zone boundary phonons. The internal T_{2g} mode was also observed to undergo a "splitting" into three components below the transition.

In our work, we have observed additional IR bands below the phase transition. These data are summarized in Table II.

We have fit several models to the data, making various assumptions as to the origins of the observed lines.

TABLE III. Frequencies calculated for various selected models, fitting the approximate observed values (in parentheses) (cm^{-1}).

Mode	$\text{K}_2[\text{SnCl}_6]$		$\text{K}_2[\text{SnBr}_6]$		$\text{K}_2[\text{TeCl}_6]$		$\text{K}_2[\text{TeBr}_6]$	
	Model 6	Model 7	Model 6	Model 7	Model 6	Model 7	Model 2	Model 3
$A_{1g}(\Gamma^{1g})\nu_1$	323.6 (324)	323.6 (324)	188.8 (190)	189.2 (190)	296.5 (297)	296.5 (297)	177.9 (177)	178.2 (177)
$E_g(\Gamma^{3g})\nu_2$	244.1 (244)	244.3 (244)	144.9 (144)	144.6 (144)	251.4 (251)	251.4 (251)	156.1 (157)	155.7 (157)
$T_{2g}(\Gamma^{5g})\nu_3$	174.5 (172)	174.3 (172)	111.9 (110)	111.3 (110)	143. (142)	146.2 (144)	103.5 (103)	103.9 (103)
$T_{2g}(\Gamma^{5g})\nu_L$	72.1 (72)	80.2 (80)	79.9 (80)	80. (80)	70.6 (70)	71.2 (72)	74.2 (74)	74. (74)
$T_{1g}(\Gamma^{4g})\nu_L$	43.2 (43)	42.2 (43)	46.1 (47)	32.6 (33)	43.5 (44)	42.8 (43)	48.1 (48)	34. (34)
$T_{1u}(\Gamma^{4u})\nu_3$	324.2 (324)	324.2 (324)	225. (225)	255. (255)	255. (255)	255. (255)	195. (195)	194. (195)
$T_{1u}(\Gamma^{4u})\nu_4$	171.8 (175)	172 (175)	122.7 (121)	122. (121)	133.4 (136)	134. (136)	109. (100.)	108.7 (110)
$T_{2u}(\Gamma^{5u})\nu_6$	115.6	115.5	72.6 (77)	73.8 (77)	101.1	106.9 (109)	70.5	72.2
$T_{1u}(\Gamma^{4u})\nu_L$	86.8 (84)	86.9 (84)	76.9 (78)	76.9 (84)	93. (92)	93.7 (92)	79. (79.)	79.4 (79)
X_3^-	113.5	113.3	78.4	75.	98.6 (97)	102.9	74.9	72.8
X_2^-	72.5 (74.8)	72.5 (74.8)	67.3 (65)	66.8 (65)	78.7	81.7	69.5	69.6
X_4^-	323.5	323.4	226.4	225.3	253.9	253.9	200.2	196.
X_4^-	178.	178.4	129.	124.7	141.4	138.7	114.3	110.9
X_4^-	52.	52.	41.9	38.7	56. (57)	54.3 (57)	41.2	37.9
X_5^-	323.8	323.8	225.6	225.	254.4	254.5	197.1	195.4
X_5^-	170.4	170.6	124.	121.7	130.2 (128)	128.8 (128)	110.6	107.8
X_5^-	118.9 (118)	119. (118)	88.	90.	106.3 (109)	109.7	84.	84.
X_5^-	85.1	91.8	78.	76.5	86.5 (87)	87.9 (87)	74.1	74.7
X_5^- TA	38.3 (42.5)	38 (42.5)	29.	28.2	42.3 (42)	42.1 (42)	26.8	27.6
ν_3 LO	327.	327.	230.9	227.7	260.1	258.9	210.	200.
ν_4 LO	185.8	186.2	132.	132.3	175.3	173.9	123.	126.
ν_L LO	129.7	129.8	111.5	113.9	117.5	115.2	107.	105.3

Only the $k=0$ and three new low temperature IR bands (74.8, 42.5, and 118 cm^{-1}) were used in the fitting. The results of our calculations are displayed in Table III and IV while the dispersion curves are shown in Fig. 3(a).

Based on these model calculations, we have made the mode identifications of Table II (right hand column). It should be observed that these identifications differ considerably from those of Pelzl *et al.*⁴

The splitting of the internal T_{2g} mode at 177 cm^{-1} can be explained as being due to the appearance of the zone boundary phonons X_3^+ and X_5^+ . This identification seems more likely, as a splitting of the internal mode would

indicate a distortion of the SnCl_6 octahedron. The two Raman lines at 104.4 and 96.6 cm^{-1} are more difficult to explain as our calculations indicate no even symmetry phonons from the points X or Γ in this region (although an L_1^+ mode occurs ~ 100 cm^{-1}). Pelzl's identifications of these modes as being due to an X_5^+ and X_3^+ component of the lattice T_{2g} mode must be in error. The X_3^+ mode is uniquely determined by symmetry and is a longitudinal component of the internal T_{2g} mode and only involves Cl motion. Because of the above, we believe these two bands (which are only observed below 150 K) to be two phonon features, a possible identification being X_4^+ + T_{1g} ($70 + 38 = 108$ cm^{-1}) and X_5^+ + T_{1g} ($58 + 38 = 96$ cm^{-1}).

TABLE IV. Force field model parameters.

	Model	K^a	F	F'	H	K_2	K_4	K_5	K_{rr}	Q_r	Q_k
$\text{K}_2[\text{SnCl}_6]$	7	1.13	0.242	-0.0242 ^b	-0.0077	0.0551	-0.00456	-0.0181	-0.0421	-0.418	1.0
	6	1.12	0.224	-0.0234 ^b	-0.00734	0.0549	-0.00438	-0.0250	-0.0421	-0.413	1.0
$\text{K}_2[\text{SnBr}_6]$	6	0.951	0.163	-0.0163 ^b	0.0071	0.0449	0.0082	-0.00793	-0.0136	-0.474	0.952
	7	0.885	0.178	-0.0178 ^b	0.0167	0.0464	0.000573	-0.00962	-0.0207	-0.411	1.0
$\text{K}_2[\text{TeCl}_6]$	7	0.954	0.124	-0.0008	0.0159	0.0695	-0.00635	-0.0400	0.222	-0.433	1.14
	6	0.976	0.115	-0.00323	0.0107	0.0693	-0.00486	-0.0406	0.223	-0.461	1.19
$\text{K}_2[\text{TeBr}_6]$	2	1.02	0.0435	-0.00435 ^b	0.0393	0.0478	0.00477	-0.0188	0.219	-0.554	1.0
	3	0.909	0.0690	-0.0069 ^b	0.0545	0.0480	-0.00076	-0.0165	0.206	-0.439	1.0

^aIn $\text{mdyne}/\text{\AA}$.

^b $F' = -F/10$.

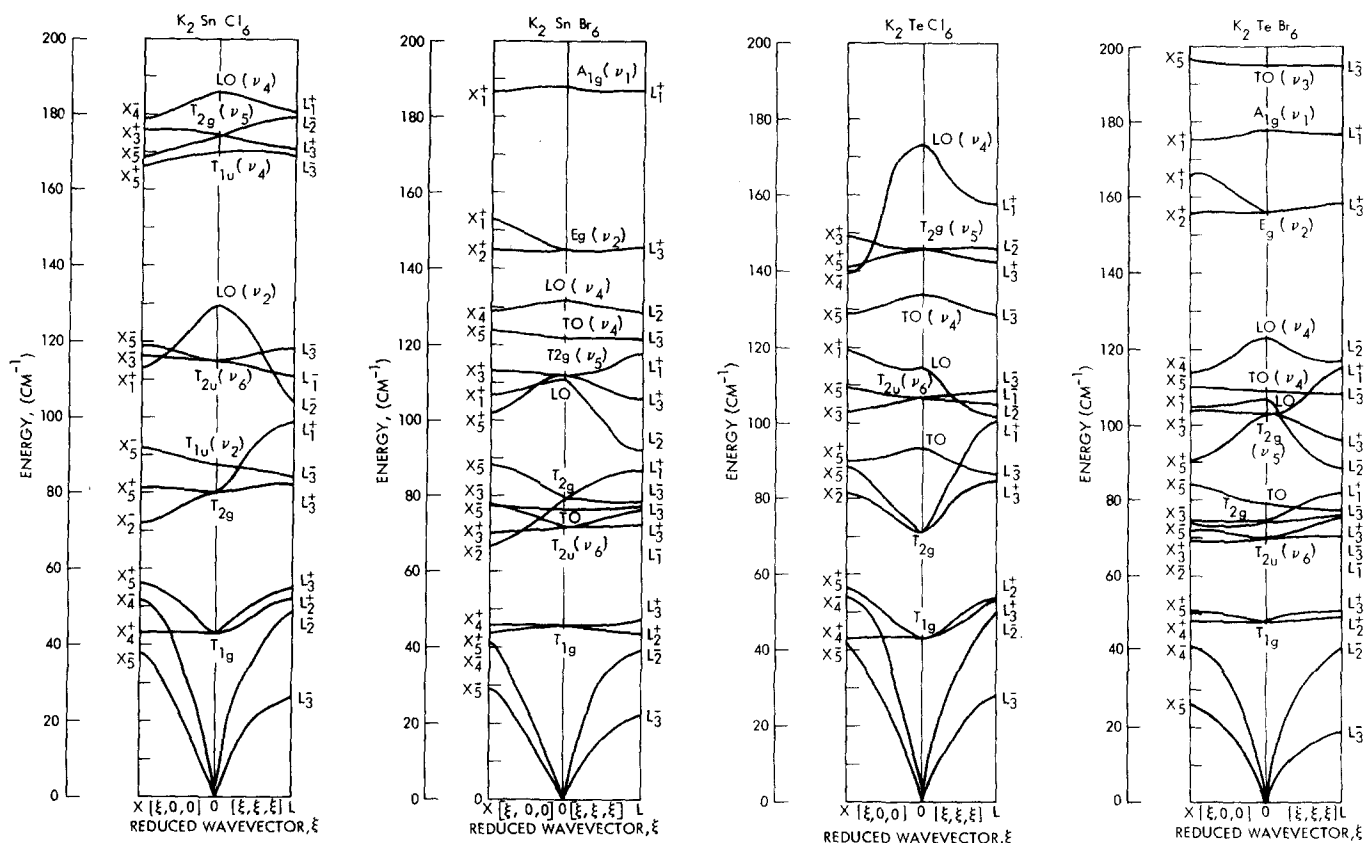


FIG. 3. Calculated dispersion curves: (a) K_2SnCl_6 (model 7), (b) K_2SnBr_6 (model 6), (c) K_2TeCl_6 (model 7), (d) K_2TeBr_6 (model 2). The parameters used were those of Table IV and the results are contained in Table V.

Our results indicate a slight separation between the T_{2g} , $k=0$ lattice mode and its X_5^+ component. We believe these to be associated with the bands at 80 and 84.5 cm^{-1} , respectively.

In our fitting of the parameters of the model, initial identifications were made using the room temperature data. Based on the dispersion curves of these early fittings, zone boundary phonons were correlated to the bands appearing in the low temperature spectra. The fits of Table III and IV are representative of this. In model 6, the T_{2g} band was placed at 72 cm^{-1} . This band is observed to shift to 80 cm^{-1} with temperature. Model 7 was run with T_{2g} at 80 cm^{-1} . This caused the X_5^- component of the T_{1u} to shift from 85 to 92 cm^{-1} (the T_{1u} was held at 84 cm^{-1}). This shift toward higher cm^{-1} corresponds to observed IR behavior in the region 74 – 98 cm^{-1} . The parameters that changed most between Model 6 and 7 were K_5 , the K–K interaction, and F and F' , the internal Cl–Cl constants. There was no calculated shift in the soft $T_{1g}(X_5^+)$ and $T_{1g}(X_4^+)$ modes. This is to be expected considering the way these parameters enter the model.

$K_2 [SnBr_6]$

From the results summarized in Table I, K_2SnBr_6 has O_h^5 symmetry above 400 K . Below this, it passes through a tetragonal phase with symmetry D_4^2 . This space group is not a subgroup of O_h^5 and cannot be reached with a distortion of symmetry of a point X phonon. Because of this, the analysis using zone boundary phonons is not

strictly valid in this case. However, it is believed that the O_h^5 zone boundary X point phonons are a good approximation to the position of D_4^2 phonons.

The temperature dependence of the data shows that T_{1u} shifts to higher energy as the temperature decreases (78 – 84 cm^{-1}). Also, the T_{2g} mode apparently shifts from 82 to 88 cm^{-1} .

The D_4^2 space group lacks inversion symmetry. Anthonson¹¹ used this to explain the low temperature Raman band at 116 cm^{-1} as being due to the T_{1u} mode. We see no other Raman band appearing in the IR.

We initially attempted to fit the room temperature data. Based on this, a low temperature IR band at 65 cm^{-1} was identified as being due to X_2^- . This was used in fit model 6. No other $k \neq 0$ phonons were used. The results of the calculation are displayed in Table III and IV, while the dispersion curves are shown in Fig. 3(b).

Without using the lack of inversion symmetry, we have identified the 116 cm^{-1} band as being the X_3^+ component of T_{2g} . Several features were accounted for as possible two phonon events. These were the 101 cm^{-1} IR band as being $X_4^+ + X_4^-$ ($57 + 42 = 99$) or X_5^- , the 88 cm^{-1} Raman band as T_{2g} or $X_4^+ + T_{1g}$ ($57 + 33 = 90$), and the 80 cm^{-1} band as T_{2g} or $T_{1g} + X_5^+$ ($33 + 47$).

$K_2 [TeCl_6]$

In fitting the data for this compound, initial attempts were made using the $k=0$ modes. As the work pro-

gressed, 13 $k=0$ and odd symmetry X point phonons were identified and used in the model. The number of parameters was increased to ten, i. e., the conditions $F' = -F/10$ and $Q_X = 1$, were not enforced.

The results of the model fitting are displayed in Tables III and IV while the phonon dispersion curves are shown in Fig. 3(c). Table II lists the final identifications based on the model. Model 7 was a special attempt to force the T_{2u} mode to the 109 cm^{-1} region.

As with the cases of $K_2[\text{SnCl}_6]$ and $K_2[\text{SnBr}_6]$, it was necessary to explain some of the features as two phonon combinations. These included the bands at 110 cm^{-1} ($T_{1g} + X_4^+ = 44 + 68$), 101 cm^{-1} ($T_{1g} + X_5^+ = 44 + 60$), and 84 cm^{-1} ($T_{1g} + T_{1g} = 44 + 44$).

This compound appears to show splitting of the lattice T_{2g} and the T_{1g} modes due to the lowered symmetry. The X_4^+ mode was picked as the band at 68 cm^{-1} due to this mode always being 5–10 cm^{-1} higher in energy than the X_5^+ .^{1,4} It should be noted that the 68 cm^{-1} band could also be due to the T_{2g} mode splitting.

$K_2[\text{TeBr}_6]$

$K_2[\text{TeBr}_6]$ has symmetry C_{2h}^5 below 405 K, a transition to a lower symmetry below 243 K is indicated by nuclear quadrupole experiments.¹⁴ The spectra of Table II shows corresponding bands in the IR and Raman (110, 100, and 55 cm^{-1}). While the possible loss of inversion symmetry cannot be ruled out, we believe it to be accidental.

Eight $k=0$ frequencies were identified and used in the models of Tables III and IV. The dispersion curve of model 2 is displayed in Fig. 3(d). Model 3 was an attempt to move the T_{1g} band to 34 cm^{-1} .

Table II shows the identification based on these models. The Raman and IR coincidences are probably due to T_{1u} and X_3^+ (X_1^+) (110 cm^{-1}), T_{2g} and $X_4^+ + X_4^-$ (100 cm^{-1}), and $X_4^+(X_5^+)$ and $T_{1g} + X_5^-$ (55 cm^{-1}). Generally, the fits and identifications for $K_2[\text{TeBr}_6]$ are the least satisfying.

CONCLUSION

The Raman and infrared spectra accompanying the phase transitions in four hexachloro- and hexabromometallates have been investigated. Where data was not available from the literature, new spectra were taken. The results of a simple lattice dynamical calculation

show that all new bands appearing in the spectra can be explained in terms of zone boundary phonons from the point X becoming allowed due to unit cell doubling. Several misidentifications appearing in previous works have been corrected.

A shortcoming of our lattice model in predicting the soft T_{1g} and X_4^+ modes has been investigated and traced to the omission of second intercell nearest neighbor interactions.

- ¹G. P. O'Leary and R. G. Wheeler, *Phys. Rev. B* **1**, 4409 (1970).
- ²H. Boysen and A. W. Hewat, *Acta Crystallogr. Sect. B* **34**, 1412 (1978); H. Boysen, J. Ihringer, W. Prandl, and W. Yelon, *Solid State Commun.* **20**, 1019 (1976); J. A. Lerbscher and J. Trotter, *Acta Crystallogr. Sect. B* **32**, 2671 (1976).
- ³J. Winter, K. Rossler, J. Bolz, and T. Pelzl, *Phys. Status Solidi B* **74**, 193 (1976); J. Winter and K. Rossler, *J. Phys. (Paris)* **37**, 265 (1976).
- ⁴J. Pelzl, P. Engels, and R. Florian, *Phys. Status Solidi* **82**, 145 (1977).
- ⁵R. G. S. Morfee, L. A. K. Staveley, S. T. Walters, and D. L. Wigley, *J. Phys. Chem. Solids* **13**, 132 (1960).
- ⁶A. Sasane, D. Nakamura, and M. Kubo, *J. Magn. Reson.* **3**, 76 (1970); K. R. Jeffry, *J. Magn. Reson.* **7**, 184 (1972).
- ⁷D. H. Brown, K. R. Dixon, C. M. Livingston, R. H. Nuttall, and D. W. A. Sharp, *J. Chem. Soc. A* **1967**, 100.
- ⁸K. Rossler and J. Winter, *Chem. Phys. Lett.* **46**, 566 (1977).
- ⁹G. Markstein and H. Nowotny, *Z. Kristallogr.* **100**, 265 (1938).
- ¹⁰E. E. Galloni, M. R. deBenyacar, and M. T. deAbeledo, *Z. Kristallogr.* **117**, 470 (1962).
- ¹¹J. W. Anthonson, *Acta Chem. Scand. Ser. A* **28**, 974 (1974); B. I. Swanson, *Phys. Status Solidi A* **47**, 95 (1978).
- ¹²G. Engell, *Z. Kristallogr.* **90**, 341 (1935).
- ¹³R. W. Berg, F. W. Poulsen, and N. J. Bjerrum, *J. Chem. Phys.* **67**, 1829 (1977).
- ¹⁴D. Nakamura, K. Ito, and M. Kubo, *J. Am. Chem. Soc.* **84**, 163 (1962).
- ¹⁵I. D. Brown, *Can. J. Chem.* **42**, 2758 (1964).
- ¹⁶S. L. Chodos, *J. Chem. Phys.* **57**, 2712 (1972); S. L. Chodos and R. A. Satten, *J. Chem. Phys.* **62**, 2411 (1975).
- ¹⁷S. L. Chodos, A. M. Black, and C. D. Flint, *Chem. Phys. Lett.* **33**, 344 (1975); *J. Chem. Phys.* **65**, 4816 (1976).
- ¹⁸S. L. Chodos, A. M. Black, and C. D. Flint, *J. Chem. Phys.* **65**, 4816 (1976).
- ¹⁹J. D. Donaldson, S. D. Ross, J. Silver, and P. J. Watkiss, *J. Chem. Soc. Dalton Trans.* **1975**, 1980.
- ²⁰D. M. Adams, J. D. Findlay, M. C. Coales, and J. S. Payne, *J. Chem. Soc. Dalton Trans.* **1976**, 371.